J Real-Time Image Proc
DOI 10.1007/s11554-011-0202-0

ORIGINAL RESEARCH PAPER

Real time cardiac image registration during respiration: a time series prediction approach

Mehdi Esteghamatian · Zohreh Azimifar · Perry Radau · Graham Wright

Received: 10 June 2010 / Accepted: 2 April 2011

Abstract Cardiac image registration is drawing attention for a range of merits in integrating and enhancing real-time (RT) images using a priori and complementary images of the myocardium, which might additionally be captured from other modalities. Myocardial stem cell delivery and radio-frequency ablation are some of the cases that could benefit from RT registration of high quality images. Unfortunately, most of these applications are of long duration, and must account in some manner for respiratory motion. Moreover, registration is not so keen as to compensate for these motions. Time series prediction techniques could compensate this shortcoming by proposing future approximate displacements caused by respiratory motion. In this study, we propose a three-stage framework for RT 2D into 3D cardiac image registration during respiration, composed of prior registration to extract the trend of respiratory motion and to calibrate a set of time series predictors for future motion prediction, as well RT registration to update estimated transform parameters. The proposed approach was validated in the course of four simulations and shows acceptable results for clinical circumstances.

Keywords Real-time · Cardiac · Image registration · MRI · Respiratory motion compensation · Time series prediction

M. Esteghamatian (✉) · Z. Azimifar
School of Electrical and Computer Engineering, Shiraz University, Shiraz, Iran
e-mail: esteghamat@cse.shirazu.ac.ir

P. Radau · G. Wright
Sunnybrook and Women's Health Sciences Centre, University of Toronto, Toronto, Canada

1 Introduction

Cardiovascular diseases are prevalent worldwide, thus therapeutic procedures are drawing considerable attention [1]. Image guidance of cardiac procedures is very beneficial in this case. Imaging for such purposes is performed using different modalities, each of which has its own pros and cons. For instance, Ultrasound is a flexible modality, but it suffers from limited imaging planes and low signal-to-noise ratio. X-ray fluoroscopy is common for cardiovascular interventional procedures, but with some associated drawbacks, such as poor soft tissue contrast and toxic radiocontrast agents. In contrast, RT magnetic resonance imaging (MRI) is considered to be an appropriate alternative for image guidance of cardiac procedures, because it has good tissue contrast, high frame rates, and the option to arbitrarily specify the imaging plane [2–4]. Unfortunately, the nature of MRI is too sensitive to patient motion, in particular for the myocardium (because of beating heart deformation and the respiratory motion [5]). To reduce such undesirable motion effects, active breathing control (ABC) should be employed [6]. This by itself is almost impossible during lengthy cardiac interventions. To address this limitation, fusion of high quality preprocedural images and RT images captured during operation could be beneficial in these circumstances.

On the other hand, there exist cardiac procedures which require catheterization and navigation with sub-millimeter precision, such as angioplasty or electrophysiological interventions [7–9]. Other cases such as regenerative effects and putative angiogenics require transferring genes or cells to the myocardium, for which a precise injection could be of much use [10, 11].

In order to overcome such difficulties, the main objective of this paper is to study the integration of the

Published online: 07 May 2011

real-time 2D MR images with pre-operative high resolution MR images acquired in breath-hold mode for only one cardiac cycle. This improves view of the therapist in 2D slices dynamically in real-time during the cardiac interventions. In others words, having the transform T between the previously captured high quality data and the RT images results in RT image fusion, and consequently RT MRI enhancement during respiration. Up to now, very few efforts have focused on RT cardiac image registration, with a number of them briefly reviewed here.

Smolikova et al. [12] carried out the first research on a similar topic. Their main objective was to study the effect of phase difference on registration accuracy using 3D prior images at breath-hold mode. They claimed that there is a clear benefit to register the RT 2D slices to a previously acquired 3D computed tomography (CT) or MR volume of the heart.

Huang et al. [13] presented a method for rapid registration of RT 3D ultrasound (US) images with dynamic 3D MR images in breath-hold mode. Their method takes advantage of ECG signals and a spatial tracking system. This study uses rigid registration because non-rigid registration causes a heavy computational burden and is thus unsuitable for RT registration. In ideal RT circumstances, the entire process including image acquisition, processing, and visualization should take at most 50ms. The authors showed that, compared to the existing methods of fusing RT 3D US with dynamic 3D MR images, their technique is the first to simultaneously address the issues of image acquisition, image processing, timing constraints, and the motion of the beating heart.

The heart displacement caused by diaphragm motion is also problematic in RT registration during respiration. Chung et al. [14] developed a method to detect spatial alignment of RT 2D slices and a prior 4D volume using contour tracking during respiration. The authors took advantage of contour tracking in RT registration. Their approach reduces displacement error from 5.2 to 1.61 mm. However, issues such as out-of-plane rotation, through-plane translation and respiration-related or non-cyclic deformations of the myocardium were not accounted for in their simulations. Also, variations in respiration period and amplitude were not considered in their research.

Cardiac respiratory motion exhibits different patterns in different conditions. This means that although the respiration behavior remains fixed in general, consecutive cycles are not exactly the same. In addition, patient drifts and variations in both respiration period and amplitude cause non-stationarity in respiratory motion [15–18]. All these problems are also common to adaptive radiotherapy, in which radiation is forced into targeting a tumor with respiration-inspired periodic motion.

Time series prediction approaches such as linear adaptive filter and extended Kalman filter (EKF) are widely used to overcome these limitations. For instance, to compensate radiation robot latency, future position of the tumor should be predicted [19–21]. There are also other approaches that take advantage of electromagnetic tracking systems for image-guided interventions which, are superior to optical tracking systems because they do not suffer from line-of-sight restriction [22–26]. Borgert et al. [27] proposed a respiratory motion compensation method based on externally placed electromagnetic sensor in combination with a motion model.

The above discussion provides the general idea and the main motivation of our proposed RT registration framework. The contribution of this work is RT cardiac image registration during respiration via time series predictors. Briefly, a periodic pattern of heart respiratory motion is measured first as a 4D time series, then a set of predictors are calibrated to predict this pattern. The predictors are then employed to speed up RT registration with such accuracy and speed superior to the current techniques.

2 Methods

2.1 RT 2D-3D registration during respiration using time series predictors

We propose an RT 2D-3D registration framework comprised of three stages (see Fig. 1):

1. *Prior registration* registering breathing 2D slice series into the high resolution breath-hold 3D prior volumes

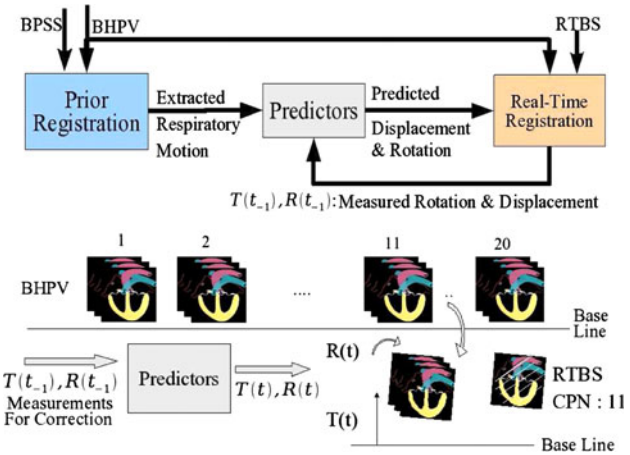

Fig. 1 *Top* framework of RT cardiac image registration during respiration. *Bottom* an RT 2D breathing slice (RTBS) with cardiac phase number (CPN) 11 is acquired; 3D volume with cardiac phase number 11 is picked up from BHPV. Initial translation $T(t)$ and rotation $R(t)$ are estimated using predictors; then RT registration is initiated

so as to extract displacement and rotation angle for each respiratory phase for several respiratory cycles.
2. *Filter parameter calibration* calibrating a set of predictors using the extracted motion from the previous stage to predict future position of the heart (displacement and rotation).
3. *RT registration* registering the breathing RT 2D slices into the high resolution breath-hold 3D priors using predictions of the filters as an initial transform and then fine tune the transform by RT registration.

2.1.1 Prior registration

This section explains how we used registration to extract cardiac respiratory motion. First, a high resolution 4D volume is captured in the breath-hold mode for one cardiac cycle with cardiac gating information, thus each 3D volume is labeled with a cardiac phase number ranging from 1 to 20. This volume is ideal and will be approximated by a set of contiguous breath-hold, gated cine MRI. Let us call this 4D volume, *breath-hold prior volumes* (BHPV). Then, a 2D slice series is acquired during free respiration, for about ten respiration cycles. It is called a *breathing prior slice series* (BPSS). Like the previous stage, we assume that each 2D slice is labeled with a cardiac phase number with temporal resolution of 83 ms (12 FPS). Finally, to extract the respiratory misalignment caused by each respiratory phase, each 2D slice of BPSS is registered into its corresponding 3D volume from the BHPV having the same cardiac phase number. As our registration transform has four parameters (3 for translation along RL, AP and CC[1] directions, respectively, and 1 for rotation), registering each pair results in a 3D vector which represents the amount of translation in three directions and a rotation angle for the corresponding respiration frame.

At the end of prior registration we have a 4D time series, consisting of a 3D vector representing the extracted respiratory displacement for each frame and its corresponding rotation angle, for ten respiration cycles. It is noteworthy that mutual information [28], as a similarity metric, is used in prior registration.

2.1.2 Filter parameter calibration

EKF and adaptive linear filters are used commonly to compensate respiratory motion for the purpose of adaptive radio therapy to target tumors [19, 29]. Same types of predictors were exploited to assess the position of heart caused by respiratory motion. Heart position is preserved in four dimensions (three for translation and one for rotation) and one predictor is used per dimension, thus we maintain four predictors. At this stage parameters of predictors are tuned by 4D motion extracted in the previous step (see Sect. 2.1.1). The 4D motion in this stage lasts ten respiration cycles to allow parameters of the predictors to converge. More cycles might be needed in general case where there is chance for disturbance in regular respiration such as irregular breathing cycles, coughing, and sneezing.

2.1.3 Real-time registration

In a RT situation a low resolution 2D slice is captured at each time step, denoted as *RT breathing slice* (RTBS). Each RTBS has a cardiac phase number (assessed from gating info). For RT registration, each RTBS is registered into its equivalent 3D volume of the BHPV with the same cardiac phase number. Initial value of the transform parameters is predicted by the predictors. Subsequently, the prior 3D image is shifted and rotated across its approximate translation vector and rotation angle, respectively. Then, the RT registration process is triggered. These predictions result in more accurate and faster convergence of transform parameter values and make RT registration feasible (see Fig. 1). Registration components are the same as prior registration step (see Sect. 2.1.1). Rigid body transform and mutual information similarity metric are exploited, and the parameters of the metric are assigned in a sense that registration converges accurately and rapidly (see Sect. 2.4).

2.2 Time series prediction for respiratory motion compensation

Time series prediction approaches have shown promising performance by effectively delivering a prescribed dose of radiation to the entire volume of a moving tumor. Murphy and Dieterich [29] and Sharp et al. [19] investigated the effectiveness of linear adaptive filter, Kalman filter and neural network in predicting the future position of a target tumor known as adaptive radiotherapy. Also, Xu et al. [30] and Ramrath et al. [21] studied the compensation for respiratory motion via EKF with promising results. Therefore, usefulness of EKF and linear adaptive filter were investigated in this study.

2.2.1 Extended Kalman filter for respiratory motion prediction

Respiratory motion has a periodic pattern very similar to sinusoidal motion making it a suitable model for respiration [31]. However, the mean, amplitude, and period of the model should be quantified dynamically due to

[1] AP: anterior–posterior, RL: right–left and CC: cranio-caudal.

non-stationary respiration. In this study we propose an EKF model based on sinusoidal behavior of the respiratory motion to assess and adjust these parameters online. A sinusoidal motion can be described using the following second-order differential equation for a 1D time series:

$$\frac{\partial^2 x}{\partial t^2} + kx = 0 \tag{1}$$

where $x = a\sin(wt) + b\cos(wt)$ and $k = w^2$. Using a state variable v, we can rewrite this second-order differential equation as a system of first-order equations:

$$\begin{cases} \frac{\partial v}{\partial t} = -kx \\ \frac{\partial x}{\partial t} = v \end{cases} \tag{2}$$

Using second-order Runge–Kutta method results in the following difference equations for calculating x_{n+1} and v_{n+1}. To take into account variation in the respiration period, k is assumed as a variable to let the model to adapt itself to the said variation. Similarly, a variable b is used to model patient drifts.

$$\begin{cases} x_{n+1} = (1 - k_n/2)x_n + v_n \\ v_{n+1} = -k_n x_n + (1 - k_n/2)v_n \\ k_{n+1} = k_n \\ b_{n+1} = b_n \end{cases} \tag{3}$$

Total state of the system at time step n is represented using vector $Y_n = [x_n \quad v_n \quad k_n \quad b_n]^{\mathrm{T}}$. To linearize the above difference equation Jacobian matrix is used as follows:

$$A_n = \begin{bmatrix} (1 - k_n/2) & 1 & -x_n/2 & 0 \\ -k_n & (1 - k_n/2) & (-x_n - v_n/2) & 0 \\ 0 & 0 & 1 & 0 \\ 0 & 0 & 0 & 1 \end{bmatrix} \tag{4}$$

Moreover, the dynamic and the measurement equations are as follow:

$$\begin{cases} Y_n = A_{n-1}Y_{n-1} + W_{n-1} \\ z_n = HY_n + u_n \end{cases} \tag{5}$$

where W_n and u_n are the process and measurement noise, respectively, and z_n is simply the summation of baseline drift b_n, sinusoidal motion x_n and measurement noise u_n, hence $H = [1 \quad 0 \quad 0 \quad 1]$. W_n and u_n are assumed to be independent of each other and normal.

$$\begin{cases} p(W) \sim N(0, Q) \\ p(u) \sim N(0, r) \end{cases} \tag{6}$$

Furthermore, to predict each direction a separate Kalman filter is employed. Consequently, four different Kalman filters are used for predicting the future position of the heart.

Kalman filter noise parameter Measurement noise covariance for translation directions is 0.5. Measurement noise covariance for rotation angle predictor is 0.04. Both values were assessed empirically in the proximity of the registration error in assessing translation and rotation angle in real-time situation. Process noise covariance for all directions were empirically observed to be the same and were equal to:

$$Q = \begin{bmatrix} 10^{-3} & 0 & 0 & 0 \\ 0 & 10^{-6} & 0 & 0 \\ 0 & 0 & 10^{-6} & 0 \\ 0 & 0 & 0 & 10^{-3} \end{bmatrix} \tag{7}$$

Additionally, initial error covariance matrix for all directions was set to a small value which is:

$$P_0 = \begin{bmatrix} 10^{-3} & 0 & 0 & 0 \\ 0 & 10^{-3} & 0 & 0 \\ 0 & 0 & 10^{-3} & 0 \\ 0 & 0 & 0 & 10^{-3} \end{bmatrix} \tag{8}$$

Convergence of the Kalman filter depends less on the error covariance. As a result, any small value in this range will have nearly similar performance.

2.2.2 *Adaptive linear filter for respiratory motion prediction*

As mentioned earlier, adaptive linear filter has been investigated in adaptive radiotherapy in which the future position of the tumor is predicted using a linear combination of previously observed positions of the tumor [19, 29], called tapped delay line. The architecture of the filter is illustrated in Fig. 2. The weights of the samples in tapped delay line (M_n) are updated using least mean square (LMS) algorithm and update formulas:

$$M_n = M_{n-1} + \mu X_n e_n \tag{9}$$

where X_n is the current tapped delay line and e_n is the error signal. The choice of parameter μ determines the

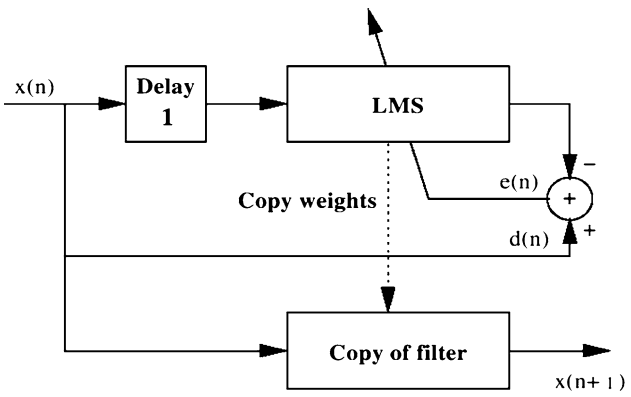

Fig. 2 Architecture of adaptive linear filter using LMS algorithm

convergence speed of the LMS algorithm. A relatively small value of μ can also ensure that the filter remains stable to the sudden changes caused by the noise.

Adaptive linear filter parameters The length of tapped delay line is a model selection parameter. Different lengths were tested ranging from 5 to 30 and, it turns out that 25 previous samples are adequate to predict a precise future position.

2.3 Experiment setup

Since registration is unsupervised, validation is a problematic stage in image registration. In other words, the ground truth values are unknown. Nonetheless, the most common method is fiducial registration error (FRE) which entails locating anatomical landmarks on both the source and target images, which is not obviously a precise method because on one hand, the apparent anatomical landmarks are not evenly distributed in our cardiac images. On the other hand, observation itself is a source of error. Consequently, we used synthetic respiratory motion to assess the tolerance of the method as precisely as possible. It also, helps us compare our approach to the method developed by our colleagues, Chung et al. [14].

Breath-hold prior volume was acquired from a human subject using a 1.5 T Signa EXCITE MR GE System with cardiac surface coil approximated by a set of contiguous, breath-hold, gated cine MRI. BHPV was acquired from FIESTA short access (SA) view (matrix size $= 256 \times 256$, slice thickness $= 5$ mm, and in-plane resolution $= 1.367$ mm $\times$ 1.367 mm), consisting of 16 slices covering the entire volume of the myocardium with cardiac gating information, consisting of 20 cardiac phases per SA slice. The BPSS and RTBS series were acquired with frame rate of 12 FPS including cardiac gating information (image matrix size $= 128 \times 128$, and in-plane resolution $=$ 2.734 mm $\times$ 2.734 mm). C++ programming language was used for registration because of algorithm efficiency and speed. The framework was tested on a PC with Intel Pentium 4 CPU 3.40 GHz and 1 GB dual channel RAM with Linux as the operating system (Kernel 2.6.24).

Interpolation method has a direct impact on the accuracy and speed of the registration process. The most popular interpolation techniques being used for image registration are nearest neighbor interpolator, linear interpolator and B-Spline interpolator. In this study, linear interpolator was used for both prior and RT registration, because first, it does not cause the computational burden of the B-spline method, and second, its interpolation accuracy is far better than that of the nearest neighbor approach.

It should also be noted that the regular step gradient descent optimizer was used in prior and RT registration processes.

Two periodic functions were used to simulate periodic respiratory motion; the first is a simple sinusoidal motion and the second one is a third-order polynomial-like periodic motion. Employing a third-order periodic motion was a deliberate choice to evaluate the strength of the predictors for non-sinusoidal periodic motions.

Four different simulations were used to evaluate the performance of the proposed predictors in different situations as described below.

1. *Varying amplitude simulation* (VA) ten smooth respiration cycles as BPSS plus five cycles of decreasing amplitude motion declining linearly from 26 to $2/3$ 26 mm with a third-order polynomial periodic motion as RTBS series.
2. *Varying oeriod simulation* (VP) ten smooth respiration cycles as BPSS plus five cycles of varying period respiratory motion ranging through 5, 4, 3, 4 and 5 s, sequentially with third-order polynomial periodic motion as RTBS series.
3. *SHort drift simulation* (SHD) ten smooth respiration cycles as BPSS plus 1.6 cycle of respiration with constant drift velocity 0.5 mm/s, all with a sinusoidal periodic motion as RTBS series (inspired from Chung et al. [14] simulation).
4. *Long drift simulation* (LD) ten smooth respiration cycles as BPSS plus ten cycles of respiration with sinusoidal drift as RTBS series with amplitude 5 mm in AP direction, all with a third-order polynomial periodic motion. Period of additive sinusoidal drift is 50 s through which drift speed reaches to the maximum of 0.63 mm/s. This periodic drift is much more complicated in comparison with the previous simulation both in terms of velocity and amplitude.

These synthetic motions are designed to simulate very common non-stationary characteristics of respiratory motion.

2.3.1 Synthetic breathing prior slice series

Statistical and geometrical heart respiratory motion was previously studied by McLeish et al. [32]. They reported 12.4 ± 5.9, 4.3 ± 3.7, and 2.0 ± 2.1 mm average translation in the CC, AP and RL directions, respectively (with the maximum translation and rotation 26 mm and 9.58°, respectively). To synthesize respiration motion, periodic translation pattern with amplitude 26 mm in direction (18.3, 8.0, 4.1 mm) along CC, AP and RL, respectively, was simulated. This is the maximum translation amplitude assessed by the authors. Also, periodic rotation pattern with amplitude 9.58° was applied. Both translation and rotation simulations reach their maximum at the same time in order to study very challenging situations. After synthesizing

respiration cyclic motion and applying this motion to BHPV, ten cycles of BPSS are synthesized by resampling slices 4, 8, and 12 (in head-to-foot direction) of BHPV in their positions before applying any synthesized translation or rotation.

In order to simulate the breathing image quality, each simulated breathing slice (any of BPSS and RTBS datasets) was resampled to half of BHPV, so image matrix size is 128 × 128 (resolution = 2.734 mm × 2.734 mm). Similarity of the synthesized RT image and the real ones was measured. Noise was assessed for both images and was obtained 0.051 ± 0.02 in RT images and 0.104 ± 0.031 gray scale values in synthetic RT images. To perform a more sophisticated simulation compared with the assumption made by Chung et al. [14], the respiration cycle period of 5 s and RT frame rate of 12 FPS were considered.

2.3.2 Acquisition and filter training time

Clinically acquiring BHPV and BPSS takes 25–30 min each including defining the short axis plane. Also, calibration of the predictors takes less than a tenth of a second (measured by *time* function in standard C programming language library) for all direction including the rotation.

2.3.3 Validation

In order to validate the performance of our proposed framework, we use *mean pixel registration error* (MPRE), which is simply the mean of differences between positions of the pixels in optimum match and the position of pixels in assessed match via registration (see Fig. 3).

$$\mathrm{MPRE}(T') = \sum_{p \in P_m} \mathrm{PRE}(p) = \sum_{p \in P_m} |T(p) - T'(p)| \qquad (10)$$

where P_m is the set of moving image pixels (RT 2D slice) in the region of the interest containing the whole

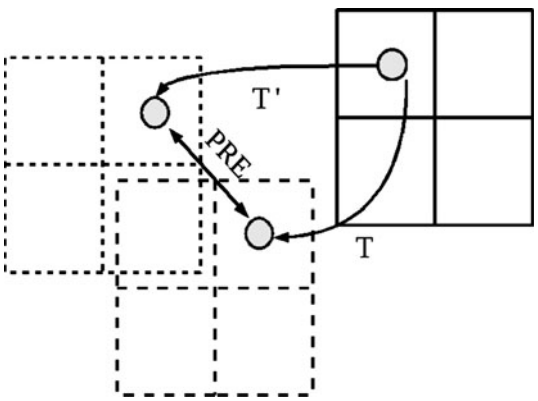

Fig. 3 Pixel registration error (PRE) is the distance between the transformed position of a pixel using optimal transform T and the calculated transform via registration T'

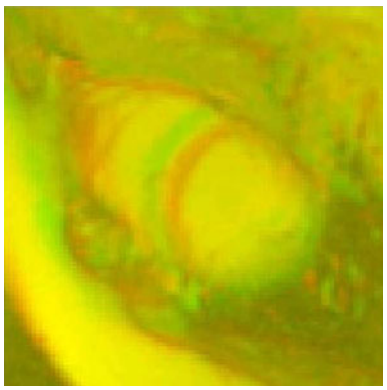

Fig. 4 Visual validation using a different color apporach. Existence of *red* or *green* pixels depicts poor registration

myocardium. An average of MPRE (AMPRE) for all time steps is calculated in order to validate the framework for each simulation.

Visual validation is performed using a different color approach in which the transformed moving image with red pixels is overlaid with the fixed image with green pixels. The resulting image would include only yellow pixels if the registration process was done perfectly, otherwise some red or green color pixels appear wherever the registration achieved poor results (see Fig. 4).

2.4 Mutual information parameter evaluation for RT registration

Amongst various algorithms, two different implementations of mutual information as a similarity metric, proposed by Mattes et al. [28] and Viola and Wells [33] have attracted the most attention. Viola's method is not fast enough for real-time purposes, because of using long tail Gaussian kernel functions. In contrast, since Mattes' method takes advantage of short tail spline functions, it can overcome the real-time challenge more effectively [28]. Moreover, parameters defined in [28] provide us with the ability to achieve the necessary accuracy and speed with respect to our problem setting. These parameters are the number of bins and the number of samples (the number of pixels utilized for mutual information) being used to measure the mutual information. To determine the best values for the parameters, we used a simple experiment in which we studied the registration time needed to reach an MPRE <0.5 mm for different bin numbers and sample numbers ranging from 30 to 70 and from 100 and 700, respectively. In the experiment, a 2D slice and a 3D volume were initially translated 3.0 mm (in 5 different random directions for each of 20 cardiac phases) and rotated for 1° from optimum match (Indeed, this initial mismatch is equal to the error of predictors in forecasting

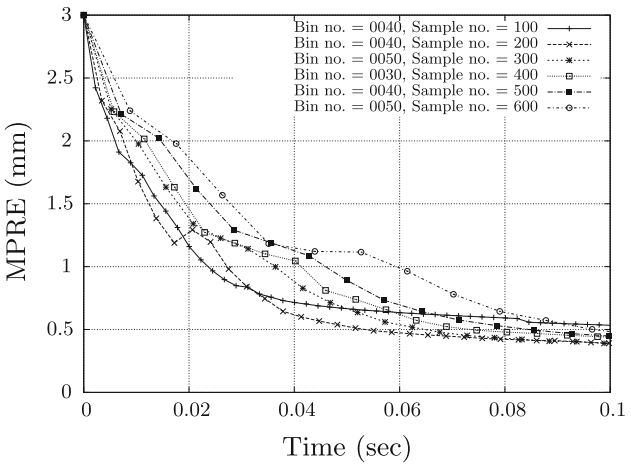

Fig. 5 Value of MPRE during registration steps for different number of samples and for the best number of bins

Table 1 Registration time (milliseconds) to reach MPRE <0.5 mm for different number of bins and different number of samples

Bin/sample	100	200	300	400	500	600
30	>200	55.0	115.0	73.5	95.4	109.6
40	117.0	53.0	69.4	80.8	84.6	112.6
50	>200	135.0	64.8	86.9	87.3	96.6
60	>200	80.0	74.2	99.5	113.7	111.2
70	>200	180.0	103.0	98.1	96.8	114.3

the heart's displacement and rotation.). Then the registration process is triggered to reach MPRE lower than 0.5 mm. Finally, the best pair of parameters are determined as being those that allow the registration process to finish in <83 ms (assuming frame rate 12 FPS for RT images). MPRE of each step in optimization process to obtain the optimum number of bins for each number of samples is plotted in Fig. 5. MPRE declines as the time advances.

According to Table 1, using 200 samples and 40 bins, the average registration time will be about 53.0 ms which is suitable for real-time registration process with frame rate 12 FPS.

3 Results

Results of four different synthetic motions proposed in Sect. 2.3 are summarized below:

- To evaluate tolerance and robustness in varying amplitude cases, VA simulation was employed for both the adaptive linear filter and the EKF model. MPRE measurements for some periods are depicted in Figs. 6 and 8 for three slices 4, 8, and 12. AMPRE during this simulation are reported in Tables 2 and 3 indicating remarkable performance in varying amplitude respirations particularly for adaptive linear filter. The different color overlay result of three slices 4, 8 and 12 using the two predictors is illustrated in Figs. 7 and 9 for visual validation.
- Robustness of the approach in varying respiration periods was studied by VP simulation. The respiration period is varied between 3 and 5 s during only five respiration cycles. MPRE for each frame during successive respiration periods 4, 3 s are illustrated in Figs. 6 and 8 for three slices 4, 8 and 12 for the two predictors. AMPRE of the five cycles of the simulation are summarized in Tables 2 and 3 for the selected slices showing that the proposed method is tolerant to variation in the respiration period. The two filters perform equally well in this simulation. A different color overlay result of three slices 4, 8 and 12 is depicted in Figs. 7 and 9.
- Comparison between presented method and in-plane contour tracking method proposed by Chung et al. [14] was inspected during SHD simulation for adaptive linear filter and the EKF model (see Tables 2, 3). Results are showing improvement in accuracy, especially for frame no. 8, and all are acceptable in a clinical condition. Note that out-of-plane rotation and through-plane translation are tolerated in the proposed framework which makes it practical and superior to contour tracking method. AMPRE of the two filters are almost the same. MPRE for some periods of the simulation is illustrated in Figs. 6 and 8 for slices 4, 8, and 12. Different color overlay result of three slices 4, 8, and 12 is also depicted in Figs. 9 and 7.
- To show robustness of our approach to more complex drift motions long drift simulation was considered. According to results (see Table 4), linear filter can predict such drifts. However, the proposed EKF model cannot predict this motion. MPRE for some periods of the simulation is illustrated in Fig. 6 for slices 4, 8, and 12. Different color overlay results of three slices 4, 8, and 12 is illustrated in Fig. 7.

MPRE is better for slice 8 through all simulations because rotation manifests itself as large translation for slices far from the rotation center. Also, MPRE has high values near the peaks of the periodic motions (frames no. 75, 105, 135, and 165 for Figs. 8a and 6a, frames no. 72, 96, 117, and 135 for Figs. 8b and 6b, frames no. 15, 45, and 75 for Figs. 8c and 6c, and frames no. 75, 105, 135, and 165 for Fig. 6d) because non-linearity increases near these moments. To put it in simpler terms, since for the EKF model, the implemented model is a linearized version of

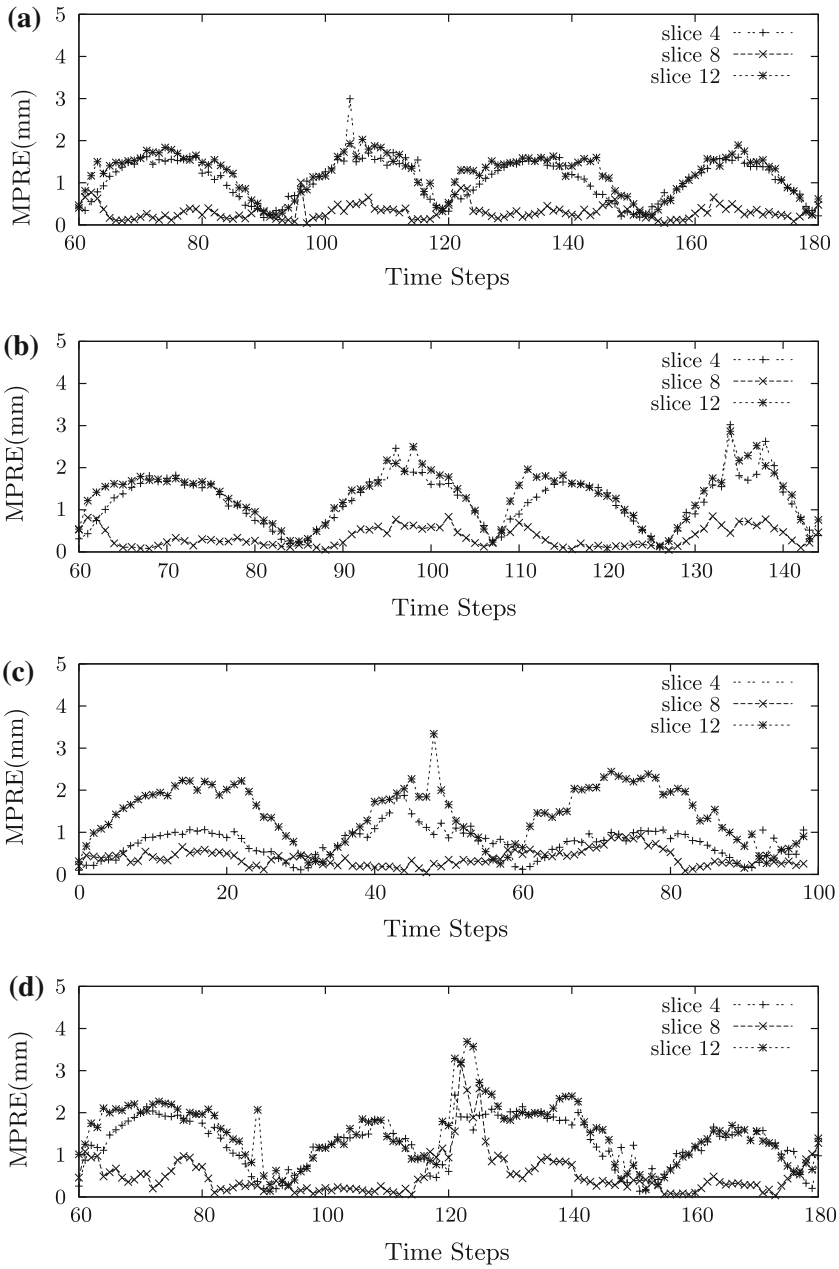

Fig. 6 **a** MPRE for adaptive linear filter for two periods (61–120 is period no. 1, 121–180 is period no. 2) of varying amplitude simulation for slices 4, 8 and 12. **b** MPRE for adaptive linear filter for two periods [61–108 is period no. 1 (4 s), 109–144 is period no. 2 (3 s)] of varying period simulation for slices 4, 8 and 12. **c** MPRE for adaptive linear filter for two periods (1–60 is period no. 1, 61–100 is part of period no. 2) of short drift simulation for slices 4, 8 and 12. **d** MPRE for two periods (61–120 is period no. 1, 121–180 is period no. 2) of long drift simulation for slices 4, 8 and 12

Table 2 Comparison between the proposed method and contour tracking method (CTM) (SHD); AMPRE for varying amplitude (VA); and varying period simulations using adaptive linear filter predictors

Simulation	VA			VP			SHD			
Slice no.:	4	8	12	4	8	12	4	8	12	CTM
AMPRE (mm)	0.98	0.31	1.19	1.52	0.54	1.39	0.78	0.38	1.15	1.61
SD (mm)	0.43	0.45	0.53	0.94	0.60	0.57	0.44	0.19	0.83	0.57
Max MPRE (mm)	3.21	3.93	4.02	2.89	3.09	3.31	3.38	0.92	4.21	3.62

Table 3 Comparison between proposed method and contour tracking method (CTM) (SHD); AMPRE for varying amplitude (VA); and varying period (VP) simulations using EKF predictors

Simulation	SHD				VA			VP		
Slice no.:	4	8	12	CTM	4	8	12	4	8	12
AMPRE (mm)	0.76	0.46	1.42	1.61	1.17	0.55	1.33	1.23	0.49	1.41
SD (mm)	0.38	0.22	0.85	0.57	0.48	0.35	0.78	0.59	0.30	0.78
Max MPRE (mm)	1.99	1.73	5.35	3.62	5.14	2.89	5.66	4.70	1.69	5.87

Table 4 Average, standard deviation and maximum for MPRE for long drift simulation (LD) using adaptive linear filter predictor

Simulation	LD		
Slice no.:	4	8	12
AMPRE (mm)	1.46	0.50	1.40
SD (mm)	1.08	0.57	1.03
Max MPRE (mm)	5.78	5.17	5.12

the original sinusoidal model and the adaptive linear filter is naturally linear, our approximated model does not perform very well in such moments.

Some limited number of large values of MPRE in graphs is the result of the divergence of RT registration process. In other words, sometimes the predicted values of the translation and rotation are not close enough to the optimum values. Therefore, the RT registration process diverges. However, since the predictors are resistant to sudden large variations, they do not affect the accuracy in the next time steps seriously.

As mentioned earlier, we used third-order polynomial describing the respiratory motions in order to assess the robustness of the proposed approach for non-sinusoidal motions. This model performed just the same as it did with sinusoidal motions. According to the results, it turned out

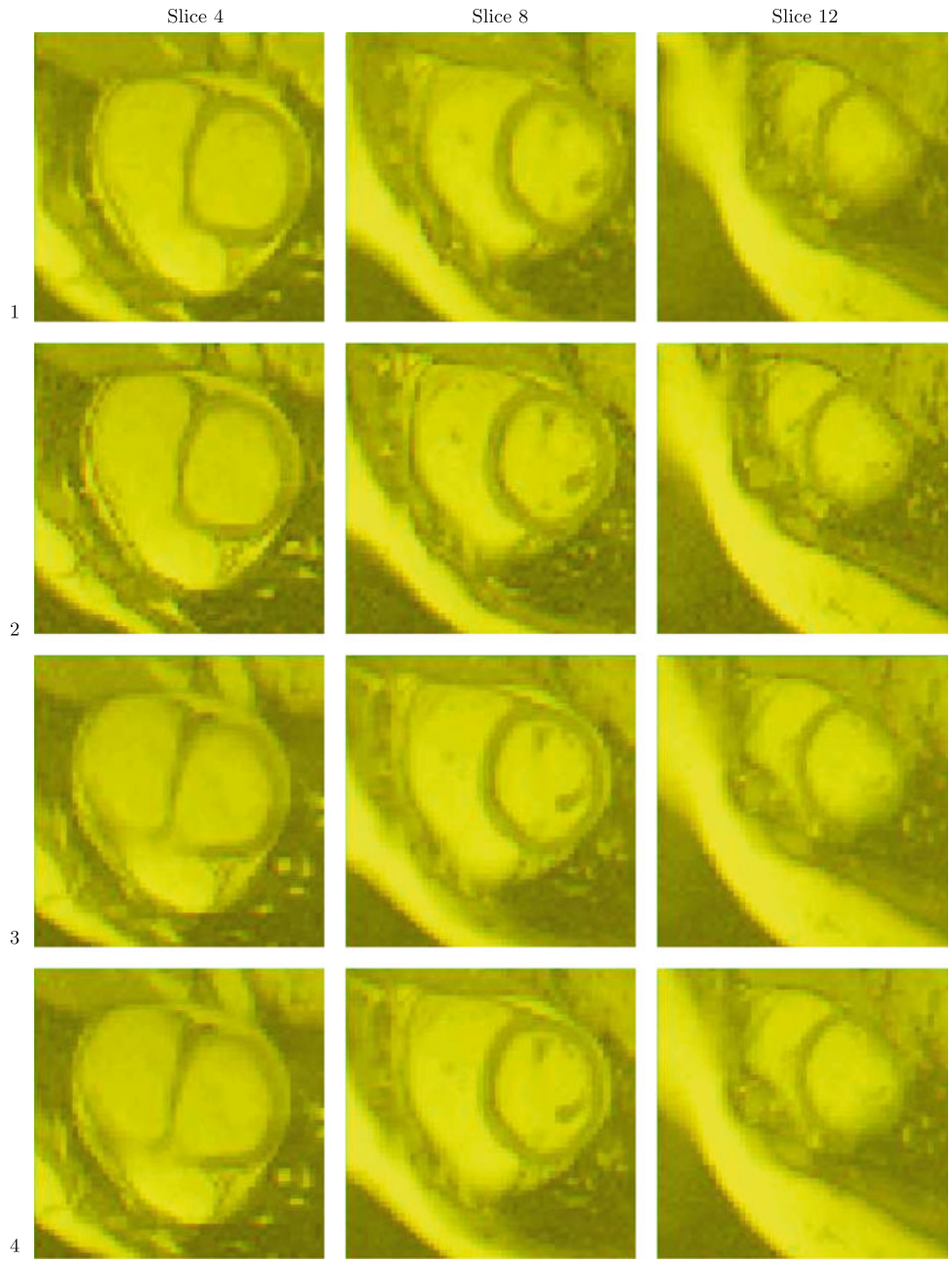

Fig. 7 Overlay result of registration for slices 4, 8, and 12 during VA simulation (*row 1*), VP simulation (*row 2*), SHD simulation (*row 3*) and LD simulation (*row 4*) for adaptive linear filter

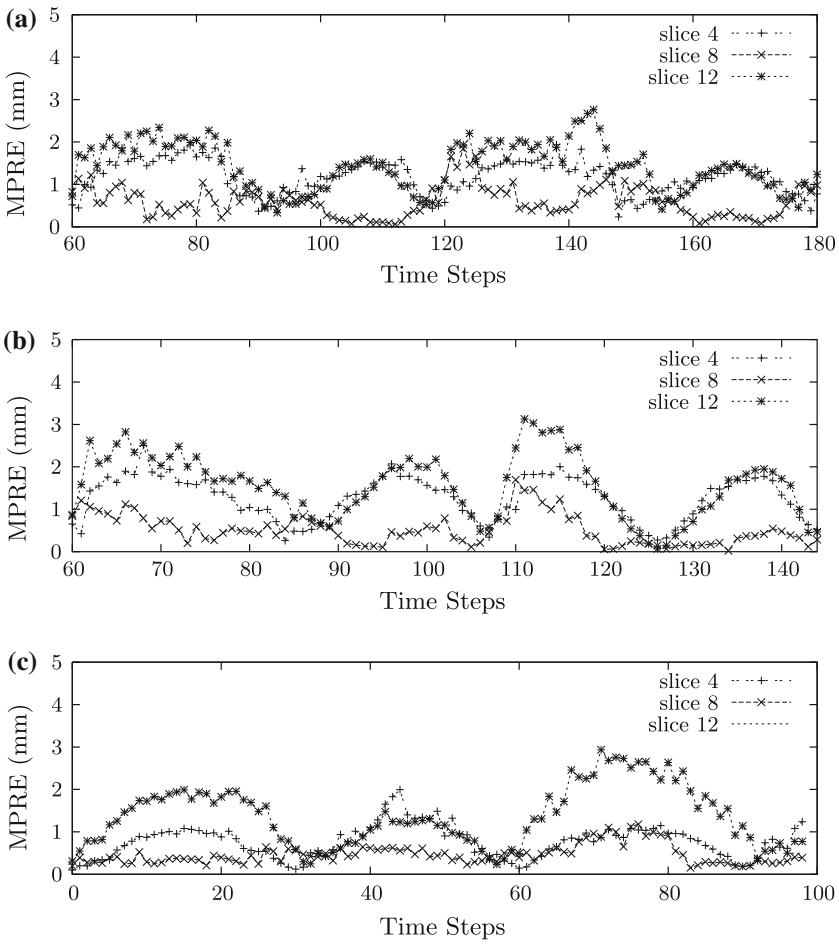

Fig. 8 **a** MPRE for EKF for two periods (61–120 is period no. 1, 121–180 is period no. 2) of varying amplitude simulation for slices 4, 8 and 12. **b** MPRE for EKF for two periods [61 108 is period no. 1 (4 s), 109–144 is period no. 2 (3 s)] of varying period simulation for slices 4, 8 and 12. **c** MPRE for EKF for two periods (1–60 is period no. 1, 61–100 is part of period no. 2) of short drift simulation for slices 4, 8 and 12

that although respiratory motion is not sinusoidal in this situation, an EKF model based on sinusoidal motion is accurate enough to let the EKF track the respiratory motion even if periodic motion is *not* essentially sinusoidal.

Note that calibration of filter parameters is completed very quickly for both predictors. Basically, the calibration time depends on the length of 4D time series extracted from pre-operative registration stage. At each time step of this 4D times series, only a handful of floating point operations are performed to adjust the parameters of both predictors. For ten cycles of respiration, it takes less than a tenth of a second to assess parameters for both adaptive linear filter and EKF which is acceptable in a clinical situation.

As the last validation step, we removed the predictors and used the rotation and translation of the previous time step as initial solution for the real-time registration. In this situation, since the difference between initial solution and optimal solution is too large, the mutual information registration could not compensate it in real-time situation (12 times per s). Subsequently, after a few time steps, the difference between pre-operative images and the their accurate position became larger and never converged again. Therefore, we took advantage of predictors so as to provide mutual information with more accurate initial solution. Consequently, mutual information could compensate the difference faster and more accurately.

4 Discussion and conclusion

In this work, we investigated the possibility of free respiration during RT cardiac MR image registration. Time series predictors were exploited to speed up RT registration in that the next position of heart is predicted. The whole process is divided into three stages: prior registration, filter parameters calibration, and RT registration. Cyclic respiratory motion is extracted during prior registration. The extracted motion is then presented to a set of time series predictors for parameter calibration. During the intervention, predictors are providing RT registration with very accurate initial solutions which shortens RT image registration at each time step. This allows the registration algorithm to bring the pre-operative MRI into alignment

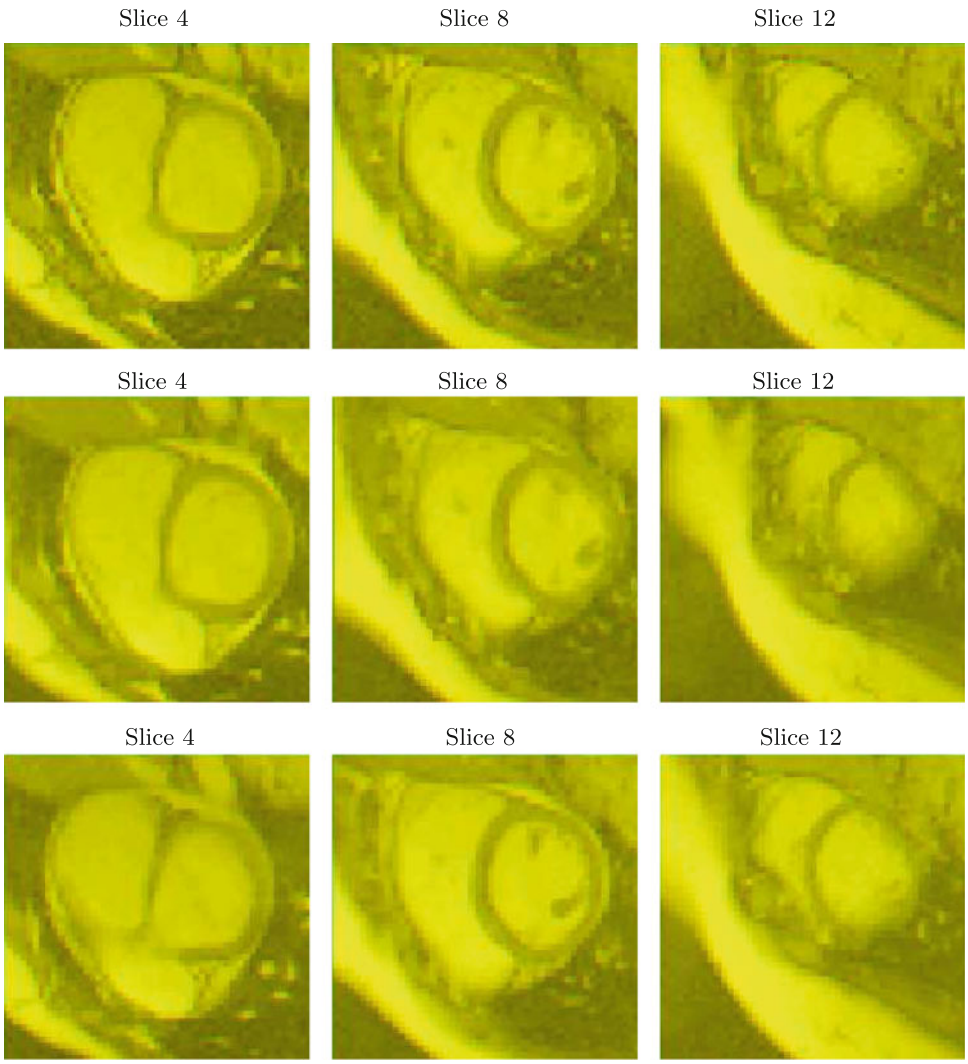

Fig. 9 Overlay result of registration for slices 4, 8, and 12 during VA simulation (*top*), VP simulation (*middle*) and SHD simulation (*bottom*) for extended Kalman filter

with the 2D RT images 12 times a second realizing RT fusion.

The proposed framework was tested using a gated 4D cardiac MR cine series, representing a complete cardiac cycle captured from a human subject in breath-hold mode. Breathing 2D slice series were synthesized to simulate four common different variations in respiration trend consisting of: Varying Amplitude Simulation, Varying Period Simulation, Short Drift Simulation, and Long Drift Simulation. In all of the simulations AMPRE is <2 mm using the proposed framework which is absolutely acceptable in clinical circumstances showing that variations in respiration amplitude, respiration period, and large drifts can be satisfactorily tolerated. Proposed framework also was compared to the contour tracking method and we observed marked improvement in results. Besides, proposed framework can tolerate out-of-plane rotation and through-plane translations in comparison with contour tracking method.

We have used EKF and adaptive linear filter to predict next position of the heart caused by respiration. Kalman filter is an optimal state estimator for linear systems, which minimizes the mean of the squared estimation error. The recursive feature of the Kalman filter makes it suitable for on-line prediction. However, for non-linear signals, model selection and model linearization affect the predictions performance. In contrast, adaptive linear filters have less model complexity so that model selection is done simply by choosing the length of tapped delay line and it has also compensated long drift simulation in comparison with EKF predictors according to our experiment results.

A single processor personal computer was used to perform on-line prediction and registration during our experiments and it is evident that working with multiple processors and parallel registration techniques [34, 35] provides more CPU time making the RT registration component more rapid and more accurate. Besides, there

are some other prediction techniques such as partial least square fitting and Fourier series model which we will consider to see how they improve the results. Also, since we plan to extend the same framework for ultrasound to MR image registration, it is inevitable to use mutual information as similarity metric. However, for sole single modality registration, improved Gauss–Newton optimization method using squared differences similarity metric [36] is a rapid registration method which potentially speeds up single modality registration using the same framework for real-time applications.

References

1. Lloyd-Jones, D., Adams, R.J., Brown, T.M., Carnethon, M., Dai, S., Simone, G.D., Ferguson, T.B., Ford, E., Furie, K., Gillespie, C., Go, A., Greenlund, K., Haase, N., Hailpern, S., Ho, P.M., Howard, V., Kissela, B., Gorelick, P., Kissela, B., Kittner, S., Lackland, D., Lisabeth, L., Marelli, A., McDermott, M.M., Meigs, J., Mozaffarian, S.D., Mussolino, M., Nichol, G., et al.: Heart disease and stroke statistics—2010 update. A report from the american heart association statistics committee and stroke statistics subcommittee. Circulation **121**, e46–e215 (2010)
2. Guttman, M.A., Dick, A.J., Raman, V.K., Arai, A.E., Lederman, R.J., McVeigh, E.R.: Imaging of myocardial infarction for diagnosis and intervention using real-time interactive MRI without ECG-gating or breath-holding. Magn. Reson. Med. **52**(2), 354–361 (2004)
3. Serfaty, J., Yang, X., Foo, T.K., Kumar, A., Derbyshire, A., Atalar, E.: MRI-guided coronary catheterization and PTCA: a feasibility study on a dog model. Magn. Reson. Med. **49**(2), 258–263 (2003)
4. Spuentrup, E., Ruebben, A., Schaeffter, T., Manning, W.J., Gnther, R.W., Buecker, A.: Magnetic resonance-guided coronary artery stent placement in a swine model. Circulation **105**, 874–879 (2002)
5. Makela, T., Clarysse, P., Sipila, O., Pauna, N., Pham, Q.C., Katila, T., Magnin, I.E.: A review of cardiac image registration methods. IEEE Trans. Med. Imaging **21**, 1011–1021 (2002)
6. Wong, J.W., Sharpe, M.B., Jaffray, D.A., Kini, V.R., Robertson, J.M., Stromberg, J.S., Martinez, A.A.: The use of active breathing control (ABC) to reduce margin for breathing motion. Int. J. Radiat. Oncol. Biol. Phys. **44**(4), 911–919 (1999)
7. Nath, S., DiMarco, J.P., Haines, D.E.: Basic aspects of radiofrequency catheter ablation. J. Electrophysiol. **5**(10), 863–876 (1994)
8. Cappato, R., Kuck, K.H.: Catheter ablation in the year 2000. Curr. Opin. Cardiol. **15**(1), 29–40 (2000)
9. Lardo, A.C., McVeigh, E.R., Jumrussirikul, P., Berger, R.D., Calkins, H., Lima, J., Halperin, H.R.: Visualization and temporal/spatial characterization of cardiac radiofrequency ablation lesions using magnetic resonance imaging. Circulation **102**, 698–705 (2000)
10. Bador, C., Brandes, C., Popp, R., Rupp, S., Urbich, C., Aicher, A., Fleming, I., Busse, R., Zeiher, A.M., Dimmeler, S.: Transdifferentiation of of blood-derived human adult endothelial progenitor cells into functionally active cardiomyocytes. Circulation **107**(7), 1024–1032 (2003)
11. Dick, A.J., Guttman, M.A., Raman, V.K., Peters, D.C., Pessanha, B.S.S., Hill, J.M., Smith, S., Scott, G., McVeigh, E.R., Lederman, R.J.: Magnetic resonance fluoroscopy allows targeted delivery of mesenchymal stem cells to infarct borders in swine. Circulation **108**(23), 2899–2904 (2003)
12. Smolikova, R., Wachowiak, M.P., Drangova, M.: Registration of fast cine cardiac MR slices to 3D pre-procedural images: toward real-time registration for MRI-guided procedures. In: Medical Imaging 2004: Image Processing, vol. 5370, pp. 1195–1205 (2004)
13. Huang, X., Hill, N.A., Ren, J., Guiraudon, G., Boughner, D., Peters, T.M.: Dynamic 3D ultrasound and MRI image registration of the beating heart. MICCAI 2005 Part I. LNCS, vol. 3749, pp. 171–178 (2005)
14. Chung, D., Satkunasingham, J., Wright, G., Radau, P.: Real-time registration by tracking for MRI-guided, cardiac interventions. Proc. SPIE **7**(30), 402–410 (2006)
15. Patil, C.P., Saunders, K.B., Sayers, B.M.: Modeling the breath by breath variability in respiratory data. In: Respiratory Control: A Modeling Perspective (Proceedings of the Oxford Conference 1988), pp. 343–352 (1989)
16. Donaldson, G.: The chaotic behaviour of resting human respiration. Respir. Physiol. **88**, 313–321 (1992)
17. Liang. P., Pandit, J., Robbins, P.A.: Non-stationarity of breath-by-breath ventilation and approaches to modeling the phenomenon. In: Modeling and Control of Ventilation, pp. 117–121 (1995)
18. Benchetrit, G.: Breathing pattern in humans: diversity and individuality. Respir. Physiol. **122**, 123–129 (2000)
19. Sharp, G.C., Jiang, S.B., Shimizu, S., Shirato, H.: Prediction of respiratory tumour motion for real-time image-guided radiotherapy. Phys. Med. Biol. **49**, 425–440 (2004)
20. Yee, P., Haykin, S.: A dynamic regularized radial basis function network for nonlinear, nonstationary time series prediction. IEEE Trans. Signal. Proc. **47**, 2503–2521 (1999)
21. Ramrath, L., Schlaefer, A., Ernst, F., Dieterich, S., Schweikard, A.: Prediction of respiratory motion with a multi-frequency based extended Kalman filter. In: Computer Assisted Radiology and Surgery (CARS 2007), pp. 27–30 (2007)
22. Wood, B.J., Zhang, H., Durrani, A., Glossop, N., Ranjan, S., Lindisch, D., Levy, E., Banovac, F., Borgert, J., Krueger, S., Kruecker, J., Viswanathan, A., Cleary, K.: Navigation with electromagnetic tracking for interventional radiology procedures: a feasibility study. J. Vasc. Interv. Radiol. **16**, 493–505 (2005)
23. Solomon, S., Dickfield, T., Calkins, H.: Real-time cardiac catheter navigation on three-dimensional CT images. J. Interv. Cardiac Electrophysiol. **8**, 27–36 (2003)
24. Solomon, S., Magee, C., Acker, D., Venbrux, D.: Experimental nonfluoroscopic placement of inferior vena cava filters: use of an electromagnetic navigation system with previous CT data. J. Vasc. Interv. Radiol. **10**, 92–95 (1999)
25. Solomon, S., White, P., Wiener, C., Orens, J., Wang, K.: Three-dimensional CT-guided bronchoscopy with a real-time electromagnetic position sensor. Chest **118**, 1783–1787 (2000)
26. Ben-Haim, S., Osadchy, D., Schuster, I., Gepstein, L., Hayam, G., Josephson, M.: Nonfluoroscopic, in vivo navigation and mapping technology. Nat. Med. **2**(12), 1393–1395 (1996)
27. Borgert, J., Kruger, S., Timinger, H., Krucker, J., Glossop, N., Durrani, A., Wood, B.J.: Respiratory motion compensation with tracked internal and external sensors during CT guided procedures. Comput. Aided Surg. **11**(3), 119–125 (2006)
28. Mattes, D., Haynor, D.R., Vesselle, H., Lewellyn, T.K., Eubank, W.: PET-CT image registration in the chest using free-form deformations. IEEE Trans. Med. Imaging **22**, 120–128 (2003)
29. Murphy, M.J., Dieterich, S.: Comparative performance of linear and nonlinear neural networks to predict irregular breathing. Phys. Med. Biol. **51**, 5903–5914 (2006)
30. Xu, S., Fichtingera, G., Taylora, R.H., Cleary, K.: 3D motion tracking of pulmonary lesions using CT fluoroscopy images for

robotically assisted lung biopsy. SPIE Med. Imaging **5367**, 394–402 (2004)
31. George, R., Vedam, S., Chung, T., Ramakrishnan, V., Keall, P.: The application of the sinusoidal model to lung cancer patient respiratory motion. Med. Phys. **32**(9), 2850–2861 (2005)
32. McLeish, K., Hill, D.L.G., Atkinson, D., Blackall, J.M., Razavi, R.: A study of the motion and deformation of the heart due to respiration. IEEE Trans. Med. Imaging **21**, 1142–1150 (2002)
33. Viola, P., Wells, W.M.: Alignment by maximization of mutual information. IJCV **24**(2), 137–154 (1997)
34. Salomon, M., Heitz, F., Perrin, G., Armspach, J.: A massively parallel approach to deformable matching of 3D medical images via stochastic differential equations. Parallel Comput. **31**, 45–71 (2005)
35. Ino, F., Ooyama, K., Hagihara, K.: A data distributed parallel algorithm for nonrigid image registration. Parallel Comput. **31**, 19–43 (2005)
36. Gonzalez, D.S., Gorriz, J., Ramirez, J., Lassl, A., Puntonet, C.: Improved Gauss-Newton optimisation methods in affine registration of SPECT brain images. IEEE Electron. Lett. **44**, 1291–1292 (2008)

Author Biographies

Mehdi Esteghamatian received his B.Sc. degree in Computer Engineering (software engineering) at Electrical and Computer Engineering School, Shiraz University, Shiraz, Fars, Iran in 2005 and the M.Sc. degree in Computer Engineering (Artificial intelligence), Shiraz University, Shiraz, Fars, Iran in 2008.

Zohreh Azimifar received B.Sc. degree in computer science and engineering from Shiraz University, Shiraz, Fars, Iran in 1994 and the Ph.D. degree in system design engineering from the University of Waterloo, Waterloo, ON, Canada, in 2005. In 2005, she was Postdoctorate Fellow in Medical Biophysics at the University of Toronto, Toronto, ON, Canada. Since 2005, she has been a Faculty Member in Computer Science and Engineering at Shiraz University. Her research interest includes Artificial Intelligence as well as statistical learning of predictive models for massive data source with particular attention in computer vision and pattern recognition.